# Individual Tree Parameters Estimation for Chinese Fir (*Cunninghamia lanceolate* (Lamb.) Hook) Plantations of South China Using UAV Oblique Photography: Possibilities and Challenges

Tian Yin, Jian Zeng, Xiaoli Zhang, *Member, IEEE*, and Xuemei Zhou

***Abstract*—Chinese fir (*Cunninghamia lanceolate* (Lamb.) Hook) individual tree parameters extraction is important for scientific forest management. However, high-precision parameters extraction by field investigation or spaceborne optical remote sensing is difficult when the forest is dense and the terrain is complex. This article proposes a framework for extracting individual tree parameters by combining low-cost and high-efficiency unmanned aerial vehicle-based oblique photogrammetry with manned airborne light detection and ranging data and explores the influence of spatial resolution on the accuracy of parameter extraction. The variable window filtering (VWF) was used to detect an individual tree. The marker-controlled watershed segmentation (MCWS) and seed region growing algorithms were used to delineate the crown. The individual tree detection using VWF based on 1 m resolution achieves precision of 80%. For the crown delineation, it is more accurate based on the 0.25 m resolution using MCWS algorithm with the detection accuracy of 65%. The results show that the proposed framework can effectively detect the tree and delineate the crown under complex terrain conditions and the optimal resolution for different parameter extraction is determined, which has important guiding significance to determine the flight parameters and reduce unnecessary data processing.**

***Index Terms*—Chinese fir plantation, individual tree, oblique photogrammetry, parameter extraction.**

## I. Introduction

CHINESE fir (*Cunninghamia lanceolate* (Lamb.) Hook) is an excellent native timber species distributed throughout the subtropical region of China [1]. With the characteristics of rapid growth and excellent material quality, Chinese fir meets human needs for timber, fuel, and other forest products. The increasing demand for timber for economic development and national investment in artificial afforestation has led to a gradual increase in the area of Chinese fir plantations [1], [2], and Chinese fir has become one of the main tree species in the complex southern plantations. Currently, the area of Chinese fir forests is $9.215 \times 10^7$ hm$^2$, accounting for 28.54% of the national planted forest area [3].

Sustainable forest management of plantations requires a timely and accurate understanding of the large-scale forest growth in order to make corresponding operational decisions [4]. Detailed individual tree parameters, such as tree number, tree height, and crown area, are not only necessary information for monitoring regeneration, quantitatively analyzing forest structure and dynamic changes, and assessing forest loss [5] but also important for the management of Chinese fir plantations. However, many Chinese fir plantations have a large planting area, and the terrain and undergrowth are complex, therefore it is difficult to conduct time-consuming and laborious field investigations [4]. In addition, some Chinese fir forests are interplanted with different tree species, which makes it extremely difficult to measure individual tree parameters. Therefore, determining an effective technique for precisely surveying the plantation resources and quickly obtaining the 3-D spatial information is important for accurate monitoring and scientific management of forest resources.

Remote sensing technology has been increasingly used to assess forest resources directly or indirectly in recent decades [6], [7]. It can complement existing ground technologies [8] and provide more representative features of the forest space under investigation using a more efficient method. Small light-weight drones, such as unmanned aerial vehicles (UAVs), are flexible, easy to operate, and moderately priced [9], [10]. UAV oblique photogrammetry and light detection and ranging (LiDAR) technologies have developed rapidly [11]. UAV oblique photogrammetry and LiDAR technologies provide high spatial and temporal resolution data and are considered a potential means for observing forest areas and conducting large-scale analyses of forest systems [4], [12], [13]. LiDAR is an active remote sensing method [14]. Laser beams can penetrate the vegetation canopy

Manuscript received August 24, 2020; accepted November 13, 2020. Date of publication November 17, 2020; date of current version January 6, 2021. This work was supported by the National Key Research and Development Program of China Project "Research of Key Technologies for Monitoring Forest Plantation Resources", Ministry of Science and Technology under Grant 2017YFD0600900. *(Tian Yin and Jian Zeng contributed equally to this work.) (Corresponding author: Xiaoli Zhang.)*

Tian Yin, Xiaoli Zhang, and Xuemei Zhou are with Precision Forestry Key Laboratory of Beijing, Beijing Forestry University, Beijing 100083, China, and also with the Key Laboratory for Silviculture and Conservation of Ministry of Education, Beijing Forestry University, Beijing 100083, China (e-mail: 18601031789@163.com; zhang-xl@263.net; 529081845@qq.com).

Jian Zeng is with the Precision Forestry Key Laboratory of Beijing, Beijing Forestry University, Beijing 100083, China, and with Key Laboratory for Silviculture and Conservation of Ministry of Education, Beijing Forestry University, Beijing 100083, China, and also with China Siwei Surveying and Mapping Technology Company Ltd, Beijing 100094, China (e-mail: 347374718@qq.com).

Digital Object Identifier 10.1109/JSTARS.2020.3038819

to obtain 3-D point clouds containing forest canopy and terrain information [15]. However, acquiring high-precision LiDAR data is expensive, especially when collecting data repeatedly in large areas. In recent years, with the development of computer vision technology, UAV oblique photogrammetry has become the main means of 3-D reality modeling and information extraction [4], [16]. However, in contrast to LiDAR, optical imaging technology cannot penetrate the canopy, so it has poor ability to provide vertical structure and terrain information [17]. Therefore, several studies have emphasized that the accurate generation of structural information from oblique photogrammetry images requires using digital terrain models (DTMs) from external sources [18]–[21]. Furthermore, oblique photogrammetry has barely been used for 3-D reconstruction in forestry surveys than buildings, because it is more difficult to model forest scenes and accurately extract the parameters by conventional algorithms, especially in complex terrain and dense canopy stands.

High spatial resolution is one of the advantages of UAV oblique photogrammetry, so a lot of publications using very high resolution UAV images on experimentation and data analysis are available. Ota *et al.* [20] used UAV images with 0.07 m resolution to generate a canopy height model for tropical forests and estimate the aboveground biomass of vegetation. Jing *et al.* [22] indicated that UAV images with 0.011 m resolution can be used to extract aquatic plant growth parameters in wetlands, and the best inversion model of above–bottom biomass was determined. Melin *et al.* [23] detected forest canopy cover by combining UAV images with 0.25 m resolution and a digital surface model (DSM) with 1 m resolution. These studies indicated that spatial resolution is especially important for accurate parameter extraction. However, high spatial resolution is likely to cause data redundancy and reduce data processing efficiency. For UAV digital aerial photogrammetry, the spatial resolution of the image is inversely proportional to the flight height, which determines the data volume and acquisition efficiency. Furthermore, in mountainous areas or areas where the terrain is highly variable, the altitude is restricted by the terrain. Is there a positive correlation between spatial resolution and parameter extraction accuracy? Even if this assumption is true, the high cost of data acquisition, the difficulty in mountainous areas, and the time required for large data processing are still critical issues. Therefore, when we use UAV data as the data source, the appropriate spatial resolution is important for determining flight parameters and reducing unnecessary processing in the data analysis process.

In this research, the UAV is equipped with an oblique photogrammetric camera to obtain images of the plantations at different angles in southern China, and manned airborne LiDAR point cloud data were used to extract the DTM. By combining these two types of data, we explore different technologies for reconstructing 3-D forest scenes and effective methods for extracting individual tree parameters under the complex terrain and high-density canopies of Chinese fir plantations, and we explore the effects of spatial resolution on accuracy. In this article, we provide solutions for data collection and information extraction using oblique photogrammetry technology to survey and dynamically monitor the Chinese fir plantations.

## II. Materials

### A. Study Area

The study area is located in the Jiepai branch farm (108°20′57″–108°21′54″E, 22°57′08″–22°58′41″N), Gaofeng state-owned forest farm in Nanning City, Guangxi Province, China (see Fig. 1), with elevation ranges from 145 to 230 m and surface slopes up to 16°. The farm is in the subtropical humid monsoon climate zone with annual average temperature and precipitation of 21.6 °C and 1300.6 mm, respectively. The red soil layer is approximately 55 cm, which is suitable for the growth of Chinese fir. The total vegetation coverage is 70%, and the forest cover is dominated by artificial forests, including Chinese fir (*Cunninghamia lanceolate* (Lamb.) Hook), yew (*Taxus chinensis*), huacai (*Manglietiastrum sinicum*), eucalyptus (*Eucalyptus robusta* Smith), and red vertebrae (*dygoxyllum*). There are also approximately 37 species of shrubs and 22 species of undergrowth herbs. The terrain of the study area is complex, and the canopy density is high. Thus, it is very challenging to accurately extract the individual tree parameters.

### B. Data Collection

*1) UAV-Based Images:* UAV-based images were collected in January 2018. Data collection consisted of two subtasks: aerial flights and ground control point placement. The images were taken with an electric multirotor UAV iHida iFly D6 [see Fig. 2(a)] equipped with an iCam Q2 oblique photogrammetric camera [see Fig. 2(b)] under windless, and sunny conditions. The iCam Q2 integrates an ortho and a side-view camera. The UAV had its own positioning system, the flight altitude is 200 m, which was determined by the image resolution. The course overlap was not less than 80%, and the side overlap was not less than 70%. Double lens oblique camera acquires the five faces images of target by swinging back and forth. The image acquisition steps are shown in Fig. 2(c), (d), and (e). First, the ortho camera acquired an image vertically 90°, and the side-view camera tilted 45° captured an image to the left [see Fig. 2(c)]. Then, the ortho camera was tilted 45° facing forward to acquire an image, and the side-view camera was not used [see Fig. 2(d)]. Finally, the ortho camera was tilted 45° facing backward to capture an image, and the side-view camera tilted 45° acquired an image to the right [see Fig. 2(e)]. Finally, four oblique and one vertical image were obtained (see Fig. 3). One flight including six routes was carried out, a total of 353 scenes of effective digital aerial images were obtained. The detailed lens and flight parameters are listed in Table I.

A real-time kinematic (RTK) global positioning system (GPS) was installed on the ground to record the position data of the control points. The UAV platform was equipped with a postdifferential postprocessing kinematic (PPK) GPS to record the approximate position data of the exposure point. The self-made control point targets were evenly placed in unobstructed, noticeable, and open areas to ensure that the control points could be clearly imaged at different shooting angles. The 3-D coordinates of all ground control points used for aerial triangulation (AT) were measured by a Tianbao differential GPS.

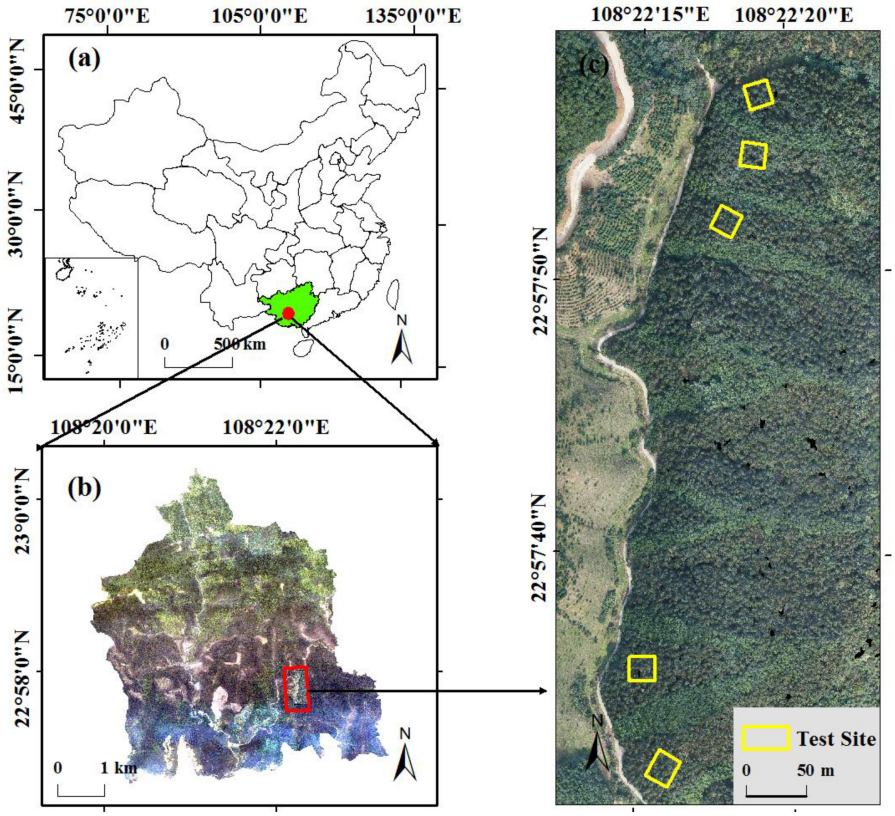


Fig. 1. Study area and the five field plot locations (CGCS2000/ 3° Gauss–Kruger CM 108E). (a) Location of Gaofeng Forest Farm, marked by the red circle. (b) Location of the study area, marked by the red rectangle. (c) Orthophoto of the study area, where the yellow rectangles show the boundaries of the five test sites.

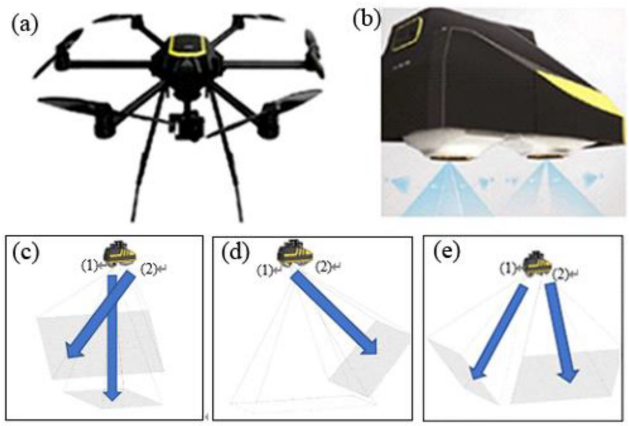


Fig. 2. Experimental drone and camera operation diagram. (a) Unmanned aerial vehicle (UAV) and (b) camera used in this study. (c)–(e) image acquisition steps. (1) ortho camera. (2) side-view camera.

Fig. 3. Four oblique and one vertical images.

The horizontal and vertical accuracy is ±0.05 m and ± 0.2 m, respectively.

During data acquisition, the oblique images may have optical distortion, which is the deviation from the control point corresponding to the images, and it needs to be corrected. In addition, it is also necessary to rotate or format the images properly according to the flight direction. The above image corrections were completed by the self-calibration before AT in Context Capture software. The detailed parameters of distortion are described in the CC user manual.

*2) LiDAR Data:* In February 2018, A Rc6-2000 UAV was equipped with a RIEGL vux-1 LiDAR sensor to acquire LiDAR data by the Chinese Academy of Forestry under windless and sunny conditions. The LiDAR data are provided in the LAS format, and the average point density is approximately 3.35 points/m$^2$. The detailed scanning and flight parameters of the airborne LiDAR system are shown in Table II.

TABLE I
UAV FLIGHT PARAMETERS

| Sensors and flight parameters | Parameter values |
|---|---|
| Sensor size（mm×mm） | 35.9×24 |
| Heading overlap（%） | 80 |
| Side overlap（%） | 70 |
| Horizontal speed（m $s^{-1}$） | 4-8 |
| Flight altitude（m） | 200 |
| Ground resolution（cm） | 3 |
| Exposure interval（s） | <4.5 |
| Focal length（mm） | 35 |
| Scanning angle (°) | 45 |
| Single camera pixel numbers (million) | 42 |

Exposure interval: the interval in which camera was triggered.
Scanning angle: the iCam Q2 integrates an ortho and a side-view camera. The angle of the side-view camera is 45°.

TABLE II
FLIGHT PARAMETERS OF AIRBORNE LiDAR

| Sensors and flight parameters | Parameter values |
|---|---|
| Laser effective scanning angle (°) | 1550 |
| Beam divergence angle (mrad) | 0.5 |
| Spot diameter (cm) | 20 |
| Width of LiDAR scanning (m) | 1040 |
| Scanning speed (r·$s^{-1}$) | 360 |
| Pulse emission frequency (Hz) | 112 |
| Flight altitude (m) | 900 |
| Flight speed (m/s) | 55 |

Laser points that are not in the actual elevation range (laser signals hit by airborne objects such as birds) are considered noise and removed to eliminate the effects of coarse points on the filtering results. The airborne laser scanning (ALS) point cloud was preprocessed by Tarascan software (www.terrasolid.com), which classified the point cloud as ground points and nonground points. A triangular irregular network (TIN) surface was created by linear interpolation of the classified ground points to construct a 1 m spatial resolution LiDAR DTM.

*3) Reference Data:* A field investigation was performed after image data collection. Five Chinese fir sample sites with dimensions of 20 × 20 m were chosen at random in the study area. We set up the base station at a stable location on the ground. The position of individual tree was measured by Sanding STS-722 tripod laser total station. The horizontal positioning accuracy is within 0.5 m. The direction and inclination of the sample sites were measured by a compass. The length of the sample site boundary was determined with a tape measure. In the sample sites, all the trees with a diameter at breast height (DBH) $\geq$ 5 cm were measured using a breast diameter ruler. A Vertex IV ultrasonic altimeter was used to measure the tree height. Due to the irregularity of the tree crowns and the steep slope of the sample sites, the measured crown area error is high, making it difficult to use the crown area as reference data for accuracy verification. Thus, we use the artificial canopy area delineated on the digital orthophoto map (DOM) as reference data for accuracy evaluation. The details are listed in Table III.

## III. METHODOLOGY

A dense point cloud with absolute coordinates was recovered from the UAV oblique images based on the structure from motion (SfM) algorithm [24]. A canopy height model (CHM) of the Chinese fir was generated by the DTM of the LiDAR data and the DSM of the oblique photographs at four spatial resolutions of 0.1, 0.25, 0.5, and 1 m. The local maximum algorithm with fixed window size (FWS) and variable window filtering (VWF) were used to detect individual treetops in the study area [25]. The boundaries of the tree crowns were delineated by the marker-controlled watershed segmentation (MCWS) and seed region growing (SRG) algorithms. Finally, the accuracy of the extraction results was evaluated. The framework is shown in Fig. 4.

### A. 3-D Reconstruction

The Bentley Context Capture V4.3 (CC) (www.bentley.com) software was used to reconstruct the 3-D model of the study area using the UAV images. Such software implements modern SfM algorithms on RGB photographs and thereby produces 3-D reconstruction models based on the location of the images [18], [25]–[28]. All the processes were fully automated. The four main steps of the workflow are as follows: select the qualified aerial images; calibrate the camera by automatically extracting the related information about the image and camera; add the GCPs; and perform AT by extracting and matching image feature points to generate dense point cloud data.

TABLE III
FIELD MEASURED RESULTS OF SAMPLE SITES

| Sample number | Number of trees | Sample size ($m^2$) | Average tree height (m) | Average crown area ($m^2$) | Average DBH (cm) | Canopy closure | Slope (°) |
|---|---|---|---|---|---|---|---|
| $S_1$ | 21 | 20×20 | 17.7 | 12.0 | 26.6 | 0.8 | 25 |
| $S_2$ | 29 | 20×20 | 16.2 | 8.7 | 22.3 | 0.8 | 24 |
| $S_3$ | 28 | 20×20 | 14.6 | 7.7 | 10.3 | 0.8 | 29 |
| $S_4$ | 22 | 20×20 | 16.2 | 9.9 | 25.4 | 0.8 | 24 |
| $S_5$ | 27 | 20×20 | 16.6 | 9.5 | 23.3 | 0.8 | 28 |

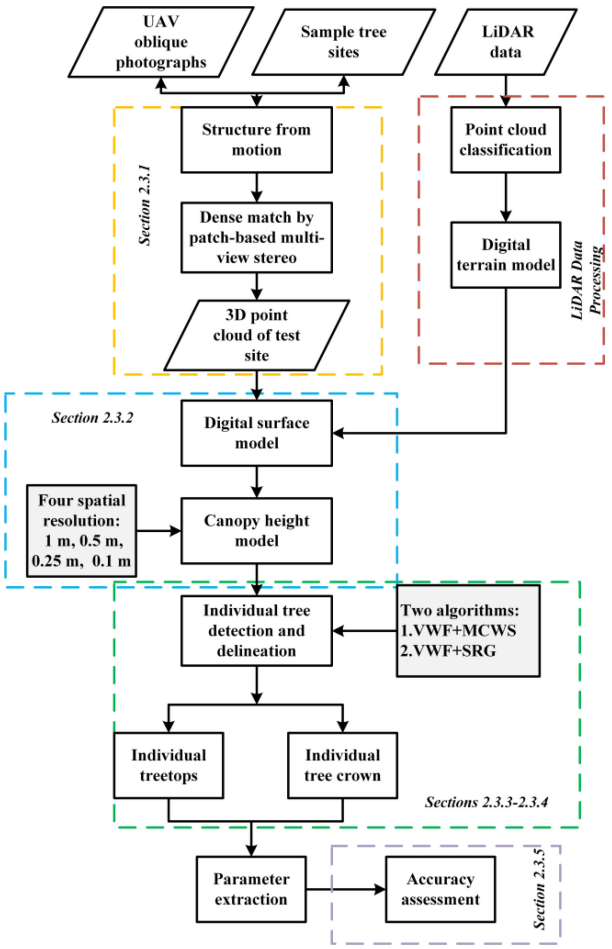


Fig. 4. Framework for 3-D parameter extraction of individual trees combining UAV-based oblique photogrammetry and airborne LiDAR data.

Detailed descriptions of this workflow can be found in this paragraph. First, the aerial images were selected to remove the unqualified images, such as unclear and color deviation images. Second, the focal length information was extracted from the images, thousands of features were detected, which were then matched between the images, and then the iterative

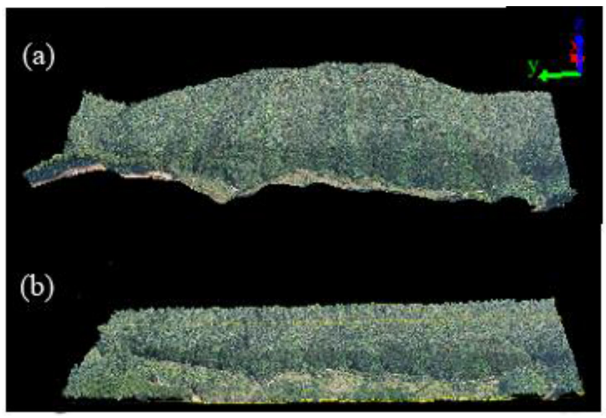


Fig. 5. Oblique photogrammetry point cloud. (a) Original dense point cloud. (b) Point cloud normalized for height.

bundle adjustment was applied to estimate the 3-D positions of the matched features, and the camera orientation and scene geometry information [29]. Third, GCPs were added for geometric precision correction to improve the accuracy of 3-D reconstruction, a nonlinear least square algorithm was used to continuously optimize and generate sparse point clouds [30]. Finally, dense matching based on a sparse point cloud is necessary to construct the 3-D information of the plantation scene. Therefore, the patch-based multiview stereo (PMVS) algorithm is used to construct the artificial forest dense point cloud [31], [32] [see Fig. 5(a)].

Next, the oblique photography point cloud is normalized to height above ground by subtracting the DTM elevation with 1 m spatial resolution generated by the LiDAR data from the Z coordinate of each point projected on the ground [25]. The normalized oblique point cloud [see Fig. 5(b)] is used to generate an oblique DSM by the GridSurfaceCreate functions in FUSION 3.4 [33].

### *B. CHM Generation*

The CHM expresses the height of the canopy surface from the ground and the horizontal distribution of the canopy. Coreg-

istration of the DSM with the DTM is a crucial step in the CHM computation because a poorly aligned DSM and DTM may produce local and overall shifts in the canopy elevation model [34]. We evenly selected 20 control points on the DSM and determined the corresponding 20 points on the DTM of the LiDAR data. The points must be obvious terrain features (road, intersections, etc.) or easily distinguishable canopy vertices. Finally, the elevation RMSE of the two layers was calculated based on the GCPs and used for elevation correction of the oblique photographs. The elevation correction error is 0.17 m. Registration of the horizontal direction was based on the affine transformation model. Finally, the CHM is calculated as the relative height between the DTM of the LiDAR data and the DSM of the oblique photographs.

Previous studies used CHM with 0.5–2 m spatial resolution to extract individual tree parameters [23], [39]. However, the Chinese fir crowns in study area can be as small as 1m, the resolution of 0.5–2 m are too coarse to describe the crown shape. Therefore, to study the influence of spatial resolution on individual parameter extraction and identify the optimal spatial resolution of CHM, we define four spatial resolutions (0.1, 0.25, 0.5, 1 m) and conduct a simulation.

### C. Individual Tree Detection

In this article, the local maximum algorithm was used for individual tree detection (ITD) based on the CHM [35], [36]. At present, the two most commonly used methods for ITD are VWF [37] and moving window with an FWS [25]. To achieve optimal tree detection, we first tested three FWSs ($5 \times 5$, $7 \times 7$, $9 \times 9$ pixels) on an unsmoothed CHM. Then, the same three FWSs were tested on a smoothed CHM by a mean smooth filter with a fixed smoothing window size (SWS) of $3 \times 3$, $5 \times 5$, and $7 \times 7$ pixels. The pixel that is the local maximum in the window is defined as the treetop, and its value is the tree height. For the VWF method, the window size changed according to the crown width (CW) to tree height (TH) allometry. The linear relationship between the CW and TH is determined from the field data ((1)) [38], [39]

$$\mathrm{CW} = \mathrm{a} \times \mathrm{TH} + \mathrm{b}. \tag{1}$$

CW is the crown width (m), TH is the tree height (m), and a and b are constants.

By applying this linear relationship to each pixel in the CHM, assuming the pixel in the CHM is a treetop, we can estimate the potential crown size by this linear relationship to set the proper window size for tree detection [40]. The pixel that is the local maximum in this window is defined as the treetop.

### D. Crown Extraction

*1) Marker-Controlled Watershed Segmentation Algorithm:* Using the accurately detected treetops as markers, we apply the MCWS algorithm to delineate the crown boundaries [41]. The CHM is first inversed so that the treetops become local minima and the crown becomes a water basin. Then, we add water to the inversed CHM, and the water rises in the basins. Finally, a dividing line is constructed at the junction of the two basins (low elevation values) to form a watershed to delineate the crown boundaries [21], [35], [42]–[44].

*2) Seed Region Growing Algorithm:* Using the accurately detected treetops as seeds, we apply the SRG algorithm to delineate the crown boundaries [45], [46]. If each original seed grows to form a continuous area, its nearest four points will be regarded as secondary seeds. If these neighbors have heights similar to that of the seed pixel, they will be included in the growth area; otherwise, they will be discarded. The above process will be repeated until all crown delineation is complete. After completing the crown delineation using the SRG and MCWS algorithms, the crown area is compared with the measured tree crown area to calculate the segmentation accuracy.

### E. Accuracy Assessment Metrics

The accuracy verification mainly includes two aspects: tree detection and crown extraction accuracy. The verification of individual-tree location detection mainly overlaps the extracted treetops with the measured treetops in ArcGIS 10.2 software. If there is only one extracted tree near the measured tree, it is positive. If there are several extracted trees, the extracted tree closest to the real position shall be taken as the positive value, and the rest are false trees. If there is no tree near the measured tree, it will be recorded as a missing tree. We use true positive (TP), false negative (FN), false positive (FP), recall (r), precision (p), and F1-score measures as accuracy indicators [47], which are calculated as follows:

$$F = \frac{TP}{TP + FN} \tag{2}$$

$$p = \frac{TP}{TP + FP} \tag{3}$$

$$F1\text{−score} = 2 \times \frac{r \times p}{r + p}. \tag{4}$$

Here, *r* describes the tree detection rate as inversely proportional to FN, therefore it can be viewed as a measure of trees detected [25]. *p* is inversely proportional to FP, indicating that treetop detection has a positive confirmation rate. The F1-score represents the harmonic mean of the detection rate and accuracy, so the higher the r and p results, the higher the F1-score.

When verifying the accuracy of the extracted crown area, the area is overlapped with the actual reference crown area delineated by ArcGIS 10.2 software. When the overlap rate for both crowns is 50% or more, we define it as correct segmentation [see Fig. 6(a)]. When it is less than 50% and the extracted crown is smaller than the reference crown, we define it as oversegmentation [see Fig. 6(c)]. Otherwise, it is defined as undersegmentation [see Fig. 6(b)]. To describe the accuracy of crown extraction, the detection accuracy (DA) ((5)) is used as an accuracy indicator [40], [48], [49]

$$DA = n/N. \tag{5}$$

Here, *n* is the number of correctly extracted crowns, and *N* is the total number of measured crowns.

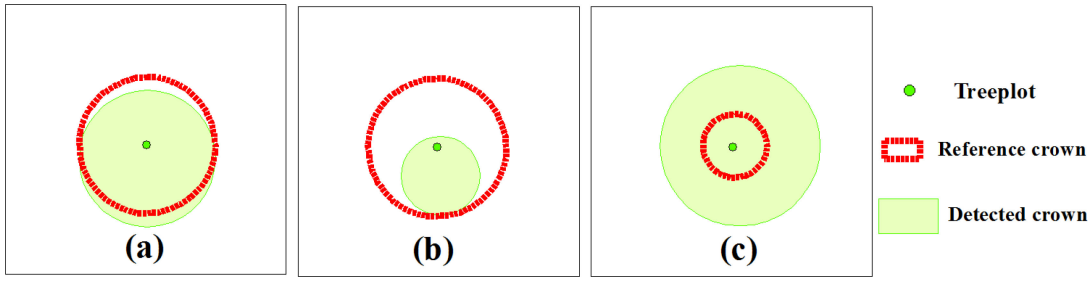


Fig. 6. Schematic of the crown segmentation results. (a) Correct segmentation. (b) Oversegmentation. (c) Undersegmentation.

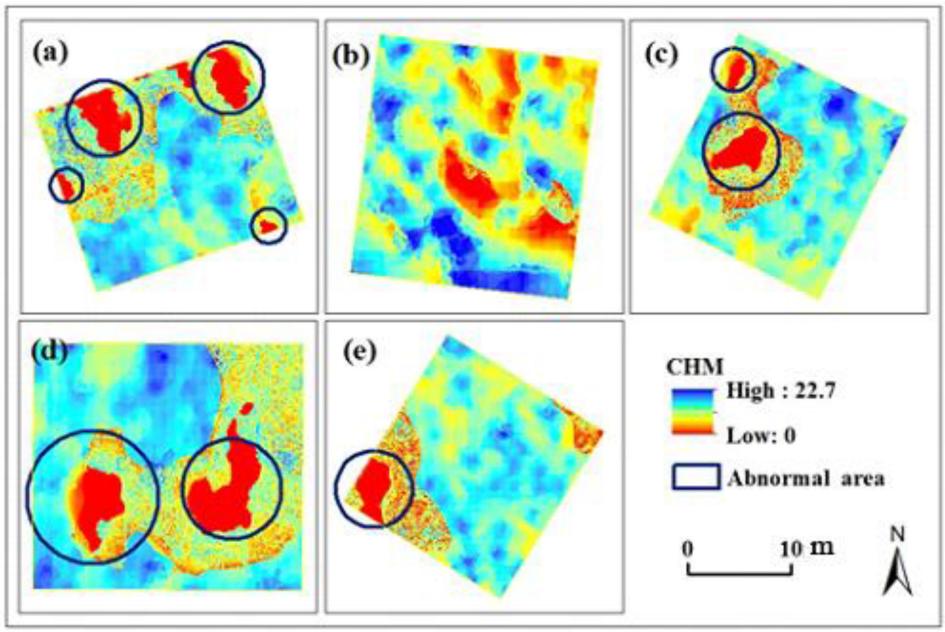


Fig. 7. Canopy height model (CHM) of the five sites at 0.1 m resolution. The abnormal areas are marked by blue circles.

In addition, we adopted four attribute precision metrics as accuracy evaluation indicators. Linear correlation analysis between the measured values and the extracted values was carried out to verify the height and crown area accuracy of individual trees. $R^2$ is used as an accuracy estimation index [50], and other estimated indicators include RMSE ((6)) [51], rRMSE ((7)) [52], and MAE (8)

$$\text{RMSE} = \sqrt{\frac{\sum_{i=1}^{n} (y_i - x_i)^2}{n}} \tag{6}$$

$$\text{rRMSE} = \frac{\text{RMSE}}{\overline{x_i}} \tag{7}$$

$$\text{MAE} = \frac{\sum_{i=1}^{n} |y_i - x_i|}{n} \tag{8}$$

where $n$ is the number of matched trees, $y_i$ and $x_i$ are the estimated value and field measured value, respectively, of the parameter, and $\overline{x_i}$ is the average value of the field measured parameter.

## IV. Results

### A. CHM Generation

Many abnormal areas are observed at the surface of the CHM (see Fig. 7) because occlusion between the crowns produces many shadow areas. These shadow areas cause a "blind spot" when the UAV is acquiring images. Therefore, many 3-D point clouds were not successfully calculated in the 3-D reconstruction process. In addition, the differing resolution between the oblique photogrammetry DSM and the LiDAR DTM results in a "sawtooth" phenomenon in the CHM (see Fig. 7). All of the above sources of error also apply to the subsequent steps.

### B. Individual Tree Detection

The detection results obtained from different FWS and SWS combinations are listed in Table IV. An FWS of 5 × 5 is more

TABLE IV
DETECTION RESULTS FOR METHOD OF FIXED WINDOW SIZE AND SMOOTHING WINDOW SIZE COMBINATIONS

| Resolution(m) | Number of field measured trees | Fix window size (FWS) | | | | | | | | | | | |
|---|---|---|---|---|---|---|---|---|---|---|---|---|---|
| | | 5×5 | | | | 7×7 | | | | 9×9 | | | |
| | | Smoothing window size (SWS) | | | | | | | | | | | |
| | | 0×0 | 3×3 | 5×5 | 7×7 | 0×0 | 3×3 | 5×5 | 7×7 | 0×0 | 3×3 | 5×5 | 7×7 |
| 0.1 | 129 | 1337 | **100** | 17 | 428 | 659 | 58 | 16 | 255 | 381 | 304 | 15 | 174 |
| 0.25 | 129 | 389 | 352 | 261 | 163 | 199 | 210 | 180 | 160 | 134 | 147 | 152 | **132** |
| 0.5 | 129 | **77** | 70 | 49 | 35 | 46 | 52 | 43 | 30 | 28 | 31 | 32 | 27 |
| 1 | 129 | **29** | 29 | 18 | 10 | 14 | 14 | 9 | 8 | 5 | 8 | 8 | 7 |

TABLE V
COMPARISON OF INDIVIDUAL TREE DETECTION OF FWS AND SWS COMBINATIONS AND VARIABLE WINDOW FILTERING

| Resolution(m) | Number of field measured trees | FWS and SWS combination | | | | | | | Variable window filtering | | | | |
|---|---|---|---|---|---|---|---|---|---|---|---|---|---|
| | | Fixed window size | Smoothing window size | Number of Extracted trees | TP | FP | FN | P | Number of Extracted trees | TP | FP | FN | P |
| 0.1 | 129 | 5×5 | 3×3 | 100 | 58 | 42 | 71 | 0.58 | 150 | 102 | 48 | 27 | 0.68 |
| 0.25 | 129 | 9×9 | 7×7 | 132 | 79 | 53 | 50 | 0.60 | 154 | **105** | 49 | **24** | 0.68 |
| 0.5 | 129 | 5×5 | 0×0 | 77 | 62 | 15 | 67 | 0.80 | 166 | 103 | 63 | 26 | 0.62 |
| 1 | 129 | 5×5 | 0×0 | 29 | 25 | 4 | 104 | 0.86 | **121** | **97** | **24** | **33** | **0.80** |

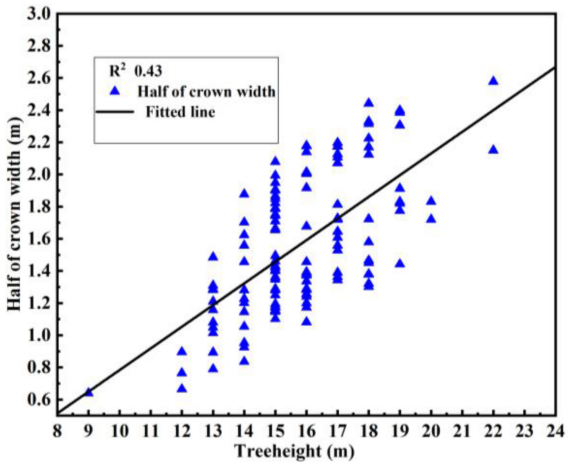


Fig. 8. Fitted line for measured tree height and half of the crown width.

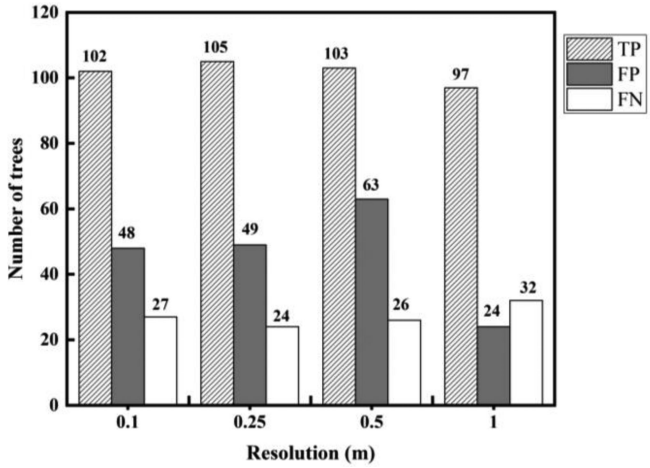


Fig. 9. Results of individual tree location detection based on variable window filtering (VWF).

accurate than that of 7 × 7 and 9 × 9. A low SWS was found to be favorable for individual tree detection. Finally, we assessed the accuracy of the best combination, which was the 5 × 5 FWS and 0 × 0 SWS combination. The detection results using VWF are shown in Fig. 10. According to the field measured results of 129 trees, the linear fitting relationship [see Fig. 8, (9)] for tree detection explains 43% of the crown size variation ($R^2 = 0.43$), which means that it can only explain 43% of the changes in window size

$$\frac{CW}{2} = 0.141TH - 0.646. \tag{9}$$

The radar plot in Fig. 10 summarizes the accuracy assessment parameters. The *r* value ranged from 0.75 to 0.81, the *P* value ranged from 0.62 to 0.8, and the F1-score value varied from 0.7 to 0.77. Among the 129 reference trees used for this article, 121 trees (see Figs. 9, 11) were detected using the CHM with 1 m resolution, and the precision was up to 80%. When the spatial resolution of the CHM was 0.25 m, the recall was up to 0.81 (see Fig. 10), indicating that the number of correctly detected trees (105) was the highest.

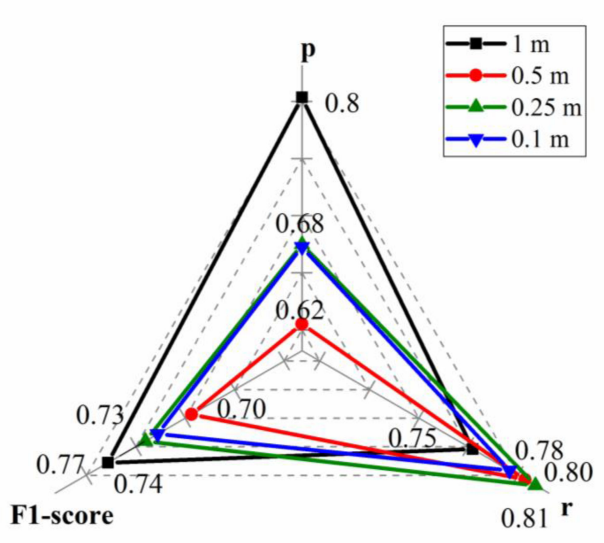


Fig. 10. Accuracy of individual tree detection based on VWF. P is the accuracy, *r* is the recall rate, and *F* is the harmonic mean of the detection rate and accuracy.

The comparison results between the FWS and SWS combinations and VWF are shown in Table V. This table illustrates that the method of FWS and SWS combinations has a precision similar to that of VWF, but there are fewer extracted treetops than measured treetops, resulting in a large amount of data loss. The precision of treetop extraction based on VWF is over 0.6, and the missed trees of this method are significantly less than those of the FWS and SWS combination method. Based on the above conditions, we conclude that the local maximum algorithm based on VWF is a useful technique for extracting individual tree locations.

### C. Tree Height Extraction Results

To assess the ability of the local maximum algorithm to extract tree height, a linear regression (see Fig. 12) is built for each group of data derived from the CHM of a certain spatial resolution. These linear regressions exhibited a strong relationship between the estimated and measured tree heights. Specifically, the three resolution models (0.1 m, 0.25 m, 1 m) have similar $R^2$ (0.65–0.76) and rRMSE (5.4%–6.9%) values, while the 0.5 m resolution model showed better results ($R^2$ = 0.82, rRMSE = 4.3%) (see Fig. 14).

### D. Crown Extraction Results

*1) Effect of Spatial Resolution on the Crown Delineation Results:* The crown delineation results are shown in Fig. 13. In general, the MCWS algorithm delineates the crowns better than the SRG algorithm. The DA of the MCWS algorithm is 3%–19% higher than that of the SRG algorithm at different resolutions (see Fig. 15), and both algorithms achieve the highest accuracy using the 0.25 m resolution CHM. No matter which delineation algorithm is used, the number of undersegmentations is higher than that of oversegmentations. For the MCWS algorithm, when the spatial resolution of the CHM is decreased from 0.1 to 1 m, the number of undersegmentations increases from 24 to 52 because the height difference is less obvious when the resolution becomes coarser. Simultaneously, the number of corresponding oversegmentations decreases from 18 to 8 because some pixels are mistakenly identified as crown boundaries.

*2) Crown Delineation Results Using Different Algorithms:* Fig. 16 shows two typical examples where the MCWS and SRG algorithms have different performance results. In Fig. 16(a), the number of crowns delineated by the SRG algorithm is much smaller than the number of reference crowns. The SRG algorithm starts growing and ends when the height changes suddenly or reaches the defined threshold, resulting in the phenomenon of oversegmentation. However, the MCWS algorithm does not stop growing until the next canopy is detected, so the height difference has less influence on it, resulting in a more accurate crown [see Fig. 16(b)]. In Fig. 16(d), the MCWS algorithm cannot detect the next crown, so canopy growth does not stop appropriately. Thus, a crown larger than the reference crown is obtained, resulting in the phenomenon of undersegmentation. The SRG algorithm stops growing the canopy when the height difference is greater than the threshold, resulting in correct segmentation [see Fig. 16(c)].

Fig. 17(a), (d), (g), (j) shows that the shape of the crown gradually changes from rounded to serrated when the spatial resolution of the CHM is reduced from 0.1 to 1 m. As the sampling interval increases from 0.1 to 1 m, the loss of detailed information in the images increases gradually. The shape of the crown changes, and the precision of crown extraction is gradually reduced. In contrast, the tree crown segmented by the SRG algorithm has no such features.

*3) Parameter Extraction Results:* A linear regression is built for each group of data derived from the CHMs of a certain spatial resolution (see Fig. 18). Various accuracy assessment metrics ($R^2$, RMSE, rRMSE, MAE) were used to compare the performances of the two crown delineation algorithms. Overall, the crown area obtained by the MCWS algorithm exhibited a better relationship between the estimated and measured crowns than the SRG algorithm. Specifically, for the MCWS algorithm, the three finer resolution groups (0.1 m, 0.25 m, 0.5 m) have slightly better $R^2$ (0.43–0.46) and rRMSE (14.4%–18.3%) (see Fig. 14) values than the 1 m resolution group ($R^2$ = 0.36, rRMSE = 22.3%). As the spatial resolution of the CHM increases from 1 to 0.1 m, the estimation accuracy also improves [see Fig. 18(a)], and the final crown area value achieves the optimal estimation accuracy at 0.1 m resolution. For the SRG algorithm, the optimal resolution is 0.25 m ($R^2$ = 0.58, rRMSE = 16.4%) [see Fig. 18(b)]. In summary, the optimal resolution and algorithm for crown delineation is 0.25 m and MCWS, respectively. The optimal resolution and algorithm for parameter extraction is 0.1 m and MCWS, respectively. However, the parameter extraction accuracy and the crown delineation accuracy should be considered at the same time because the parameter accuracy is assessed according to the correctly delineated crown [53]. Therefore, although the 0.1 m resolution model shows great potential for parameter extraction, 0.25 m is the optimal resolution for crown extraction.

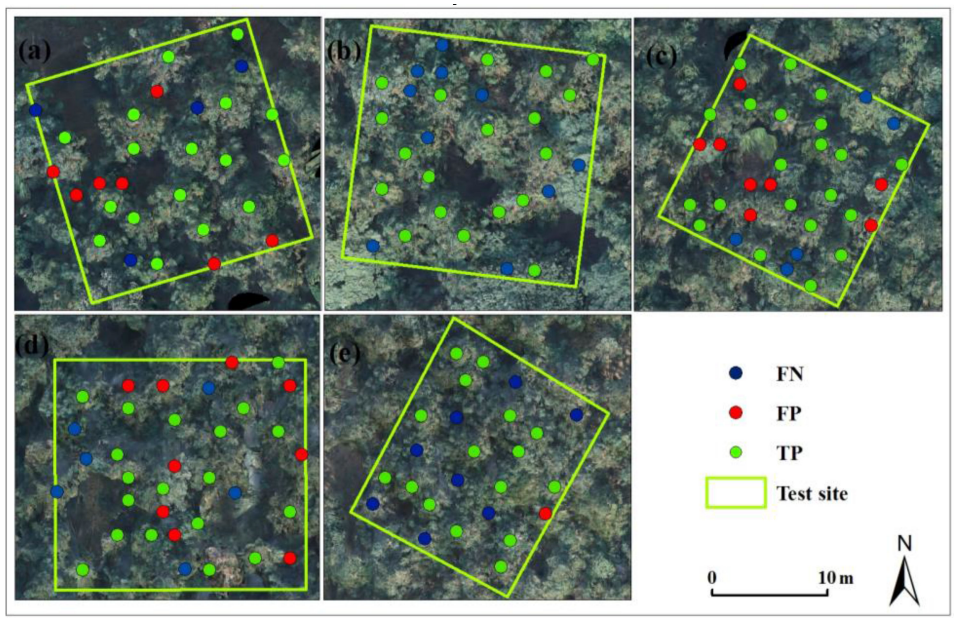


Fig. 11. Individual tree detection result of the 1 m resolution CHM based on variable window filtering. (a), (b), (c), (d), and (e) represent sample sites S1–S5, respectively; FN is false negative; FP is false positive; and TP is true positive.

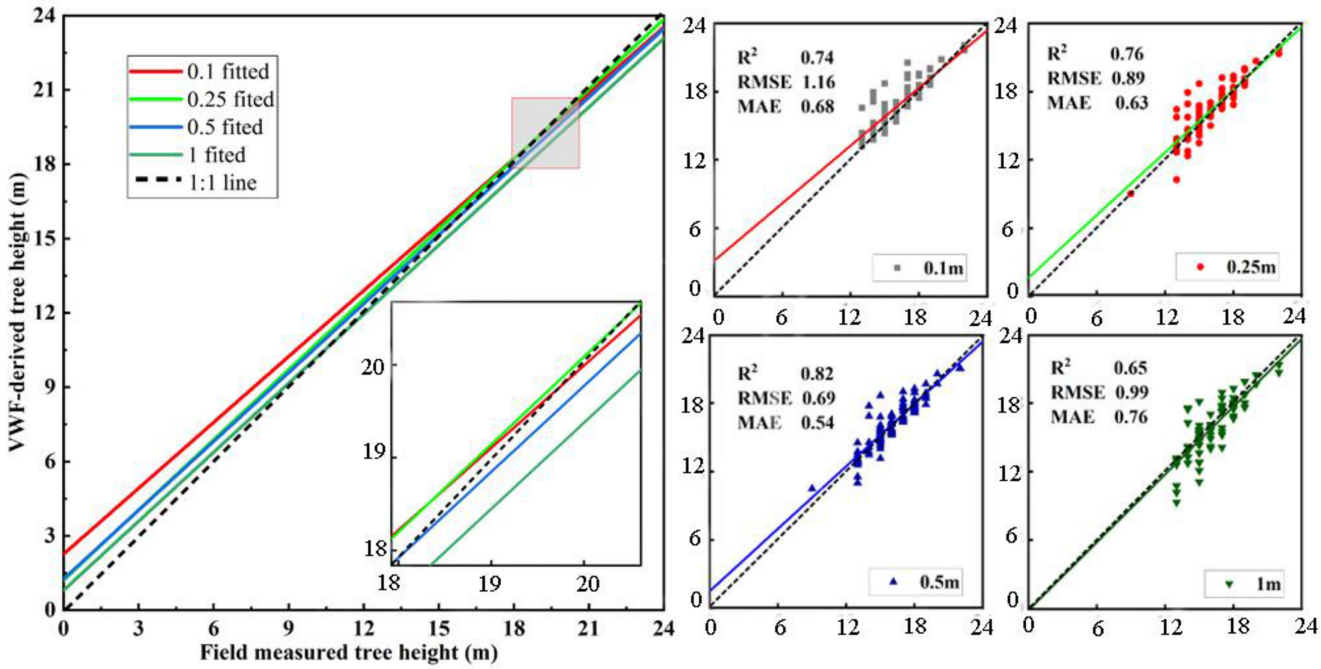


Fig. 12. Tree height extraction results. The fitted lines are plotted together on the left, and scatter plots of each spatial resolution model are plotted separately on the right.

## V. Discussion

### A. Individual Tree Detection

The VWF method detects the location of individual trees better than the method of FWS and SWS combinations because VWF determines the size of the variable window mainly depending on the relationship between tree height and crown width, thereby avoiding the limitation of the fixed window in the process of ITD. The capability of ITD is also sensitive to the FWS and SWS combinations. However, in this experiment, the point cloud density obtained by the UAV images is high enough to easily reflect the tree details; extracting treetops via a

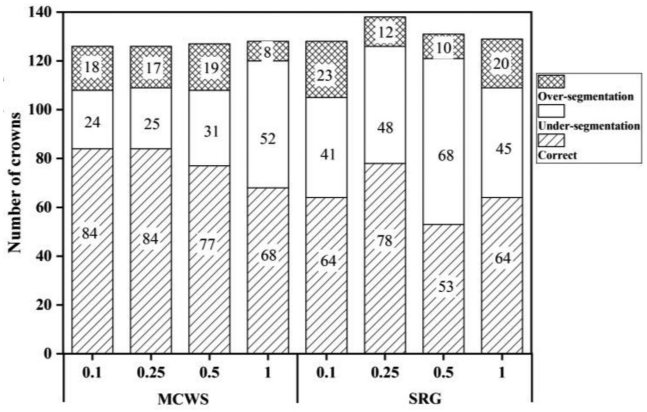


Fig. 13. Tree crown extraction results of the MCWS and SRG algorithms.

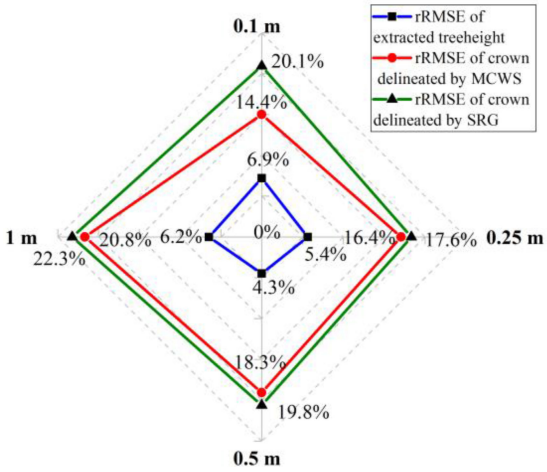


Fig. 14. Radar plot showing the detection-related RMSE of tree height and crown area.

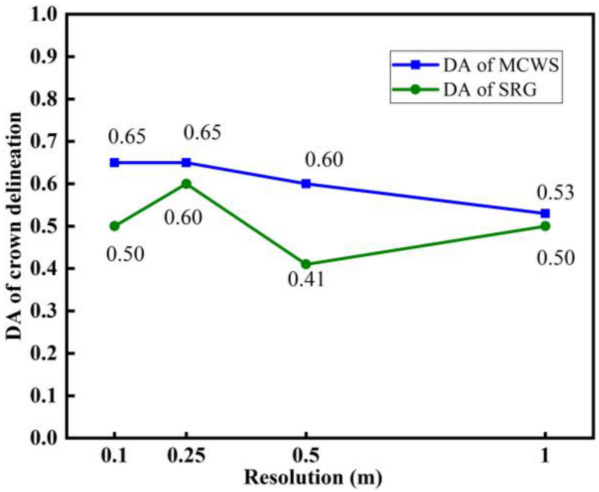


Fig. 15. Detection accuracy (DA) of the crown delineation.

smoothing window will result in detail loss and many missed trees. Therefore, the method of VWF is useful for extracting the structural parameters of plantation forests with similar structures.

The individual tree extraction results derived from CHMs with different spatial resolutions are different. Thus, we use DSMs with four different resolutions (0.1, 0.25, 0.5, 1 m) and a LiDAR DTM with 1 m resolution in the process of generating the CHMs. The CHM calculated by the DSMs with 0.1, 0.25, and 0.5 m resolutions and the LiDAR DTM with 1 m resolution has slightly lower accuracy than the CHM calculated by the 1 m resolution DSM and 1 m resolution LiDAR DTM because the former generates a "sawtooth" phenomenon. Therefore, ITD by the CHM with unmatched resolution identifies some pixels as treetops, resulting in a large number of falsely detected trees and affecting the detection accuracy. In addition, the number of missed trees is lower than that of falsely detected trees in this experiment because the point cloud generated by the SfM algorithm has high density; when resampling according to different distances, the loss of information is lower, and the retention of tree details is higher.

As the tree height is directly extracted from the CHM with different resolutions generated by the DSM and DTM, the height error comes from the resolution of the CHM, DSM, DTM, or all three. Due to the small number of ground points used during collection of the LiDAR data, a large part of the study area is generated by interpolation. In some cases, the understory covers the low vegetation, so the generated terrain is slightly higher than the real terrain. In order to improve the DTM accuracy, a higher density LiDAR point cloud is required. In addition, some error originates from the DSM. Sufficient feature points cannot be extracted for some trees because the crown is too small, or the leaves are scarce. After dense matching, the point cloud still does not contain enough points to be rasterized into a continuous point cloud, which led to the DSM error.

### *B. Individual Tree Crown Extraction*

The MCWS algorithm grows in the vertical direction [54], while the growth curve of the Chinese fir crown is steep and has much important information in this direction. Therefore, the MCWS algorithm is more suitable for individual tree crown delineation in the Chinese fir region. Using the MCWS and SRG algorithms, more crowns are undersegmented than oversegmented. The main reason for this result is the insufficient detection of treetops, because both algorithms find crown boundaries based on the correctly detected treetops. The key to correctly detect the treetops is to correctly define the window sizes [55], [56], [57], [58], [59]. In this article, variable window size was used according to the CW to TH allometry, which has proved useful for ITD in Section IV-B. However, only 43% of the CW variation is explained for the Chinese fir (see Fig. 8), which means that it can only explain 43% of the changes in window size. Determining how to explain the remaining variation and improve the detection accuracy of individual trees under high crown closure and complex terrain conditions is a substantial

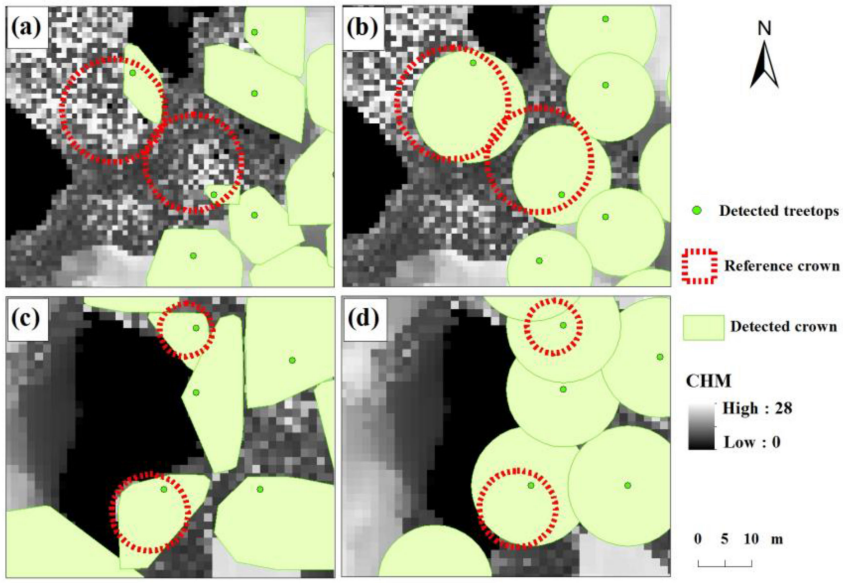


Fig. 16. Different representations of canopy segmentation by the SRG and MCWS algorithms. (a) Oversegmentation by SRG. (b) Correct segmentation by MCWS. (c) Correct segmentation by SRG. (d) Undersegmentation by MCWS.

challenge. In particular, when the resolution is 1 m, the accuracy of the SRG algorithm for crown delineation is better than that of the MCWS algorithm. The reason for this result is that a large number of missed trees are extracted by the CHM with 1 m resolution (see Fig. 11), while the SRG algorithm can determine the correct crown size by setting appropriate growing parameters when a tree is underdetected [60], which reduces the amount of undersegmentation compared to that of the MCWS algorithm. Thus, the SRG algorithm is more accurate than the MCWS algorithm.

One of the main reasons for the error is the abnormal area caused by the 3-D reconstruction process mentioned in Section IV.A (see Fig. 7). The abnormal areas have invalid data, which cause many errors in the crown delineation process. However, in this experiment, we did not attempt to solve this problem, which led to the unsatisfactory crown delineation results. In subsequent research, we will explore some methods to solve this problem and then delineate the crown again.

Another reason for the error is that the spatial information below a certain threshold height is masked during the algorithm execution, which causes the partial crown delineation to be small. Thus, scholars believe that spectral information provided by high-resolution images is more reliable than spatial information that can be masked [61]. In addition, the registration of images and LiDAR data will produce geographic errors. This experiment uses a low-density LiDAR point cloud, so the DTM generated by LiDAR has low precision and will cause crown distortion during normalization of the oblique point cloud. Furthermore, during acquisition of the UAV images (Section II.B.1)), the study area lacked obvious features (roads, intersections, etc.). Thus, self-made targets were used as control points, and manual placement of the control points will cause errors.

In addition, sample surveys may have errors, which depend on ground survey conditions and personnel. It is difficult for Vertex IV to observe the true treetops when the trees are high and the stand is dense. At the same time, the reference crown area is obtained by ArcGIS visual interpretation of the DOM image, and there will be errors in the crown area drawn by different personnel.

### C. Challenges of Using Oblique Photogrammetry for Extracting Individual Tree Parameters

Traditional remote sensing technology, satellite and aerial photogrammetry technology need manual or semiautomatic acquisition to obtain the surface texture of the image and achieve 3-D reconstruction based on high resolution images. But these technologies have serious occlusion problems, the cost of acquiring texture data is high, the data processing is complicated, the efficiency is low. LiDAR can penetrate the vegetation canopy to obtain the 3-D point cloud, which contain forest crown and terrain information. But the LiDAR data cannot obtain the RGB and texture information, and the equipment is more expensive than others. Oblique photography can acquire images from multiple angles, and obtain complete and accurate texture data and spectral features of the forest, which make up for the shortcomings of other technologies. However, there are still some obstacles in the study of parameter extraction of Chinese fir trees by oblique photogrammetry.

1) Accurate measured data are indispensable for verifying the accuracy of the estimated parameters. However, the measured data may be inaccurate due to some objective or subjective factors during data acquisition. In the future, on the one hand, the data collection process should avoid these factors to improve the data quality; on the other hand, terrestrial laser scanning (TLS) data can be used as supplementary ground data.

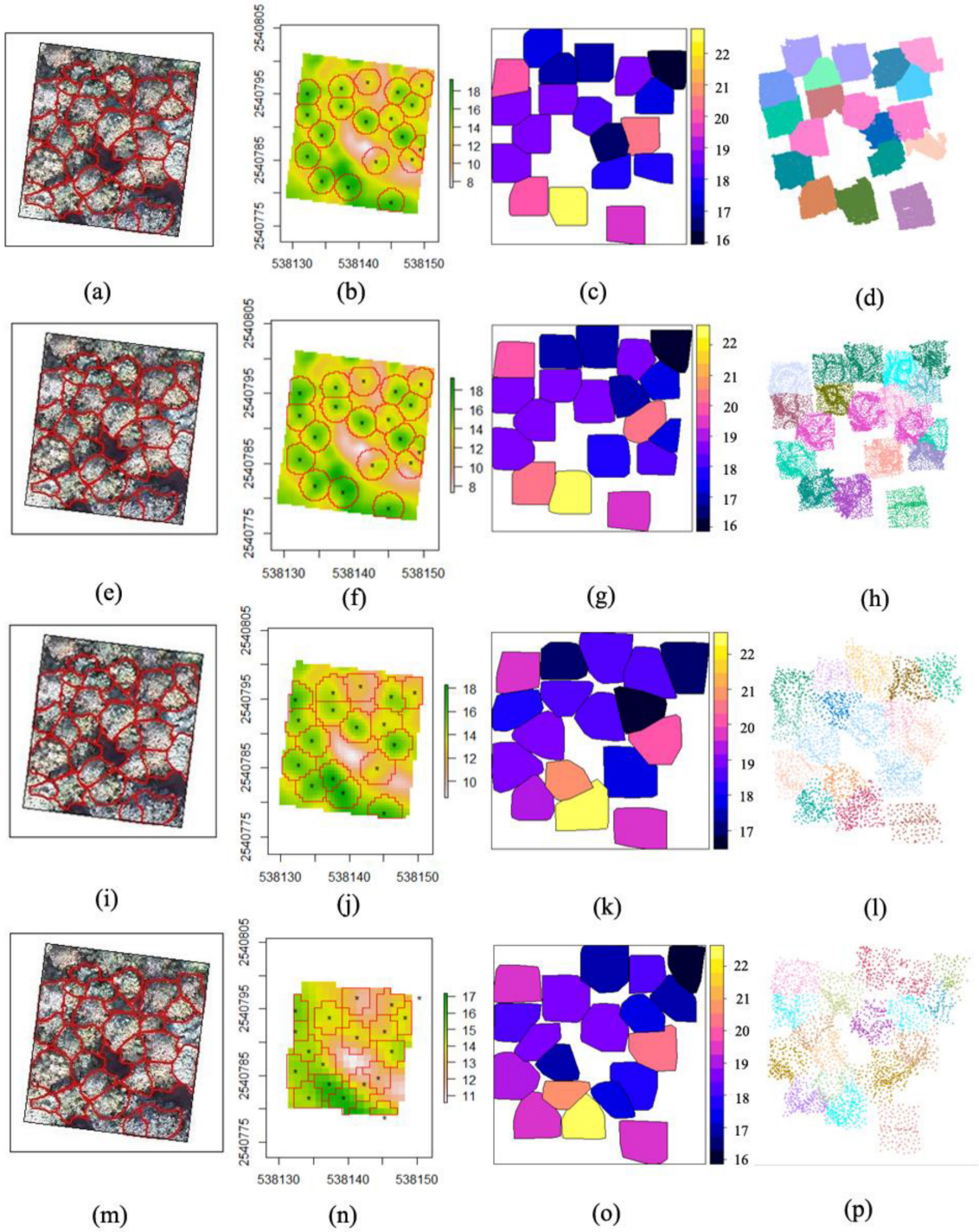


Fig. 17. Crown delineation results of the MCWS and SRG algorithms. (a), (e), (i), (m) Reference crown. (b), (f), (j), (n) MCWS results based on the CHM with 0.1, 0.25, 0.5, and 1 m resolution, respectively. (c), (j), (k), (o) SRG results based on the CHM with 0.1, 0.25, 0.5, and 1 m resolution, respectively. (d), (h), (l), (p) SRG point cloud based on the CHM with 0.1, 0.25, 0.5, and 1 m resolution, respectively.

2) The CHM used in this research is produced by the oblique photogrammetry DSM and the LiDAR DTM. Determining how to improve the accuracy of the LiDAR DTM and reduce the errors of the DSM to achieve accurate registration of the two datasets is a problem worth of further investigation.

3) The 3-D reconstruction algorithm cannot handle weak texture or the reconstruction problem of absent texture and highlighted areas. Occlusion between the crowns produces many shadowed areas, resulting in many abnormal areas in the 3-D reconstruction process of the study area, which has a substantial impact on the extraction of individual

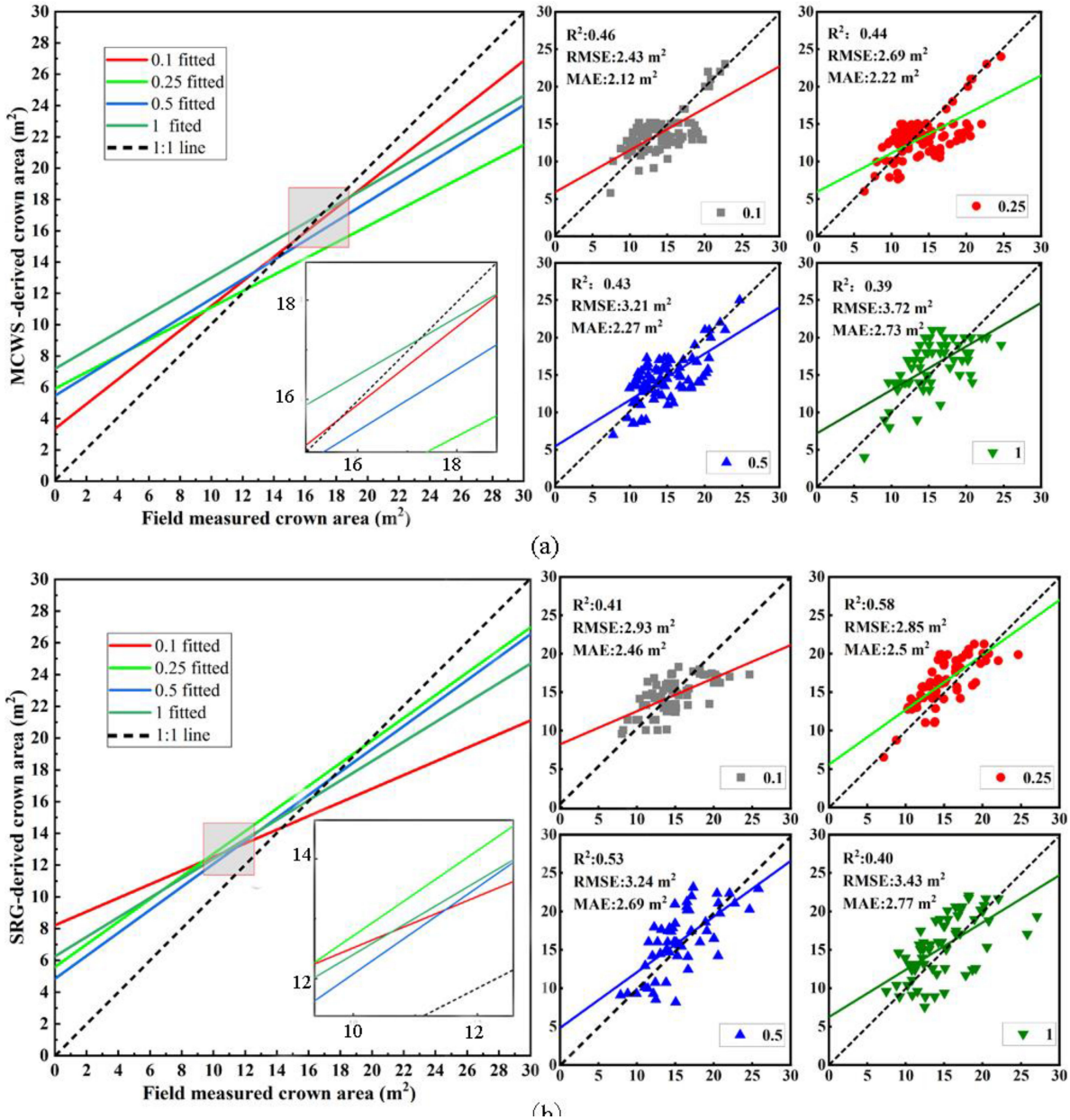


Fig. 18. Tree crown extraction results. The fitted lines are plotted together on the left, and scatter plots of each spatial resolution are shown separately on the right. (a) MCWS results. (b) SRG results.

tree parameters. In future research, we are committed to exploring suitable algorithms to extract individual tree parameters by repairing abnormal areas.

## VI. Conclusion

In this research, we extracted the structural parameters of individual trees in Chinese fir plantations by combining UAV-based oblique photogrammetry images and airborne LiDAR point cloud data and explored the influence of spatial resolution on the accuracy of parameter extraction. Then, we proposed an optimized UAV-based oblique photogrammetry framework for achieving precise forestry surveys.

1) Using computer vision theory, an incremental SfM algorithm is combined with high-precision control point data to reconstruct a 3-D point cloud from oblique images. Then, a DTM derived from LiDAR data was used to normalize the oblique photogrammetric-measured CHM, and the individual tree parameters were extracted based on the optimal algorithms. The result shows that the accuracy of individual tree detection using the VWF local maximum method at 1 m resolution is up to 80%. The individual tree height estimates achieved good accuracy with $R^2$, RMSE, rRMSE, and MAE of 0.82, 0.69 m, 4.3%, and 0.54 m, respectively, when using the 0.5 m resolution CHM. The crown area extraction is more accurate based on the 0.25 m resolution CHM using the MCWS algorithm, with RMSE, rRMSE, MAE, and DA of 2.69 $m^2$, 16.4%, 2.22 $m^2$, and 65%, respectively.

2) By comparing the parameter extraction results for CHMs with different resolutions, we concluded that spatial resolution and parameter extraction accuracy are not necessarily positively correlated, and the optimal resolution of individual tree position,

tree height, and tree canopy extraction for Chinese fir plantations is 1, 0.5, and 0.25 m, respectively. For UAV oblique photogrammetry, the spatial resolution of the image is inversely proportional to the flight altitude, and the flight altitude is the basis of UAV route design. So, these results are important for determining flight parameters and provide a guide for the acquisition of oblique photogrammetry data in the Chinese fir plantation area.

3) Compared with the traditional remote sensing technology, the proposed technical framework can provide a more efficient solution for obtaining precise surveys and monitoring Chinese fir plantations.

## ACKNOWLEDGMENT

The authors would like to thank Lin Zhao, Zhengqi Guo, Xuemei Zhou, Xiaomin Tian, and Linghan Gao from Beijing Forestry University and Prof. Erxue Chen and Dr. Lei Zhao from the Institute of Forest Resource Information Techniques CAF for their help with the field work.

## REFERENCES

[1] X. Zhang, A. Duan, and J. Zhang, "Tree biomass estimation of Chinese fir *(Cunninghamia lanceolata)* based on Bayesian method," *PLoS One*, vol. 8, Nov. 2013, Art. no. 79868.

[2] M. Zhao, W. Xiang, C. Peng, and D. Tian, "Simulating age-related changes in carbon storage and allocation in a Chinese fir plantation growing in southern China using the 3-PG model," *Forest Ecol. Manage.*, vol. 257, pp. 1520–1531, Dec. 2009.

[3] J. Lei, *Chinese Forest Resources.* Beijing, China: China Forestry Publishing House, , pp. 154–196.

[4] D. Gatziolis, J. F. Lienard, A. Vogs, and N. S. Strigul, "3D tree dimensionality assessment using photogrammetry and small unmanned aerial vehicles," *PLoS One,* vol. 10, Sep. 2015, Art. no. 137765.

[5] D. A. Kwak, W. K. Lee, J. H. Lee, G. S. Biging, and P. Gong, "Detection of individual trees and estimation of tree height using LiDAR data," *J. Forest Res.*, vol. 12, pp. 425–434, Oct. 2007.

[6] X. Hu, W. Chen, and W. Xu, "Adaptive mean shift-based Identification of individual trees using airborne LiDAR data," *Remote Sens.*, vol. 9, Feb. 2017, Art. no. 148.

[7] N. Jayaraju and J. A. Khan, "Remote sensing and geographical information as an aid for land use planning and implications to natural resources assessment: Case study, South India," in *Developments in Soil Classification, Land Use Planning and Policy Implications*. Berlin, Germany: Springer Dordrecht, Jan. 2013, pp. 577–590.

[8] M. C. Hansen *et al.*, "High-resolution global maps of 21st-century forest cover change," *Science*, vol. 342, pp. 850–853, Sep. 2013.

[9] F. Dario and R. J. Tree, "Science, technology and the future of small autonomous drones," *Nature*, vol. 521, pp. 460–466.

[10] K. Liu, X. Shen, L. Cao, G. Wang, and F. Cao, "Estimating forest structural attributes using UAV-LiDAR data in Ginkgo plantations," *ISPRS J. Photogramm.*, vol. 146, pp. 465–482, Nov. 2018.

[11] J. C. White *et al.*, "Remote sensing technologies for enhancing forest inventories: A review," *Can. J. Remote Sens.*, vol. 42, pp. 619–641, Jul. 2016.

[12] S. Martin-Alcon *et al.*, "Combining aerial LiDAR and multi-spectral imagery to assess post-fire regeneration types in a Mediterranean forest," *Can J. Forest Res.*, vol. 45, pp. 856–866, Jul. 2015.

[13] J. C. White, P. Tompalski, N. C. Coops, and M. A. Wulder, , "Comparison of airborne laser scanning and digital stereo imagery for characterizing forest canopy gaps in coastal temperate rainforests," *Remote Sens. Environ.*, vol. 208, pp. 1–14, Apr. 2018.

[14] J. M. Vilbig, V. Sagan, and C. Bodine, "Archaeological surveying with airborne LiDAR and UAV photogrammetry: A comparative analysis at Cahokia Mounds," *J. Archaeological Sci., Rep.*, vol. 33, Jul. 2020, Art. no. 102509.

[15] W. Chen, H. Xiang, and K. Moriya, "Individual tree position extraction and structural parameter retrieval based on airborne LiDAR data: Performance evaluation and comparison of four algorithms," *Remote Sens.*, vol. 12, Feb. 2020, Art. no. 571.

[16] C. Zhang and J. M. Kovacs, "The application of small unmanned aerial systems for precision agriculture: A review," *Precis. Agric.*, vol. 13, pp. 693–712, Jul. 2012.

[17] L. Cao, H. Liu, X. Fu, Z. Zhang, X. Shen, and H. Ruan, "Comparison of UAV LiDAR and digital aerial photogrammetry point clouds for estimating forest structural attributes in subtropical planted forests," *Forests*, vol. 10, no. 2, pp. 1–26.

[18] J. P. Dandois and E. C. Ellis, "High spatial resolution three-dimensional mapping of vegetation spectral dynamics using computer vision," *Remote Sens. Environ.*, vol. 136, pp. 259–276, Jun. 2013.

[19] J. Lisein, M. Pierrot-Deseilligny, S. Bonnet, and P. Lejeune, "A photogrammetric workflow for the creation of a forest canopy height model from small unmanned aerial system imagery," *Forests*, vol. 4, pp. 922–944, Nov. 2013.

[20] T. Ota *et al.*, "Aboveground biomass estimation using structure from motion approach with aerial photographs in a seasonal tropical forest," *Forests*, vol. 6, pp. 3882–3898, Oct. 2015.

[21] L. Wallace, A. Lucieer, and C. S. Watson, "Evaluating tree detection and segmentation routines on very high-resolution UAV LiDAR data," *IEEE Trans. Geosci. Remote Sens.*, vol. 52, pp. 7619–7628, Dec. 2014.

[22] R. Jing, Z. Gong, W. Zhao, R. Pu, and L. Deng, "Above-bottom biomass retrieval of aquatic plants with regression models and SfM data acquired by a UAV platform—A case study in Wild Duck Lake Wetland, Beijing, China," *ISPRS J. Photogramm.*, vol. 134, pp. 122–134, Dec. 2017.

[23] M. Melin, L. Korhonen, M. Kukkonen, and P. Packalen, "Assessing the performance of aerial image point cloud and spectral metrics in predicting boreal forest canopy cover," *ISPRS J. Photogramm.*, vol. 129, pp. 77–85, Jul. 2017.

[24] J. Lisein, M. Pierrot-Deseilligny, S. Bonnet, and P. Lejeune, "A photogrammetric workflow for the creation of a forest canopy height model from small unmanned aerial system imagery," *Forests*, vol. 4, pp. 922–944, Nov. 2013.

[25] M. Mohan *et al.*, "Individual tree detection from unmanned aerial vehicle (UAV) derived canopy height model in an open canopy mixed conifer forest," *Forests*, vol. 8, Sep. 2017, Art. no. 340.

[26] D. Turner, A. Lucieer, and L. Wallace, "Direct georeferencing of ultrahigh-resolution UAV imagery," *IEEE Trans. Geosci. Remote Sens.*, vol. 52, no. 5, pp. 2738–2745.

[27] G. Verhoeven, "Taking computer vision aloft-archaeological three-dimensional reconstructions from aerial photographs with photoscan," *Archaeol Prospect.*, vol. 18, pp. 67–73, Jan. 2011.

[28] B. U. Meinen and D. T. Robinson, "Mapping erosion and deposition in an agricultural landscape: Optimization of UAV image acquisition schemes for SfM-MVS," *Remote Sens. Environ.*, vol. 239, Jan. 2020, Art. no. 111666.

[29] M. I. A. Lourakis and A. A. Argyros, "SBA: A software package for generic sparse bundle adjustment," *ACM Trans. Math. Softw.*, vol. 36, pp. 1–30, Mar. 2009.

[30] X. Zhou and X. Zhang, "Individual tree parameters estimation for plantation forests based on UAV oblique photography," *IEEE Access*, vol. 8, pp. 96184–96199, Jun. 2020.

[31] N. Haala and M. Rothermel, "Dense multi-stereo matching for high quality digital elevation models," *Photogramm. Fernerkun.*, vol. 4, pp. 331–344, Aug. 2012.

[32] C. Stone, M. Webster, J. Osborn, and I. Iqbal, "Alternatives to LiDAR-derived canopy height models for softtree plantations: A review and example using photogrammetry," *Australian Forestry*, vol. 79, pp. 1–12, Oct. 2016.

[33] K. Kraus and N. Pfeifer, "Determination of terrain models in wooded areas with airborne laser scanner data," *ISPRS J. Photogramm. Remote Sens.*, vol. 53, pp. 193–203, Jun. 1998.

[34] H. Huang, P. Gong, X. Cheng, N. Clinton, and Z. Li, "Improving measurement of forest structural parameters by co-registering of high-resolution aerial imagery and low-density LiDAR data," *Sensors*, vol. 9, pp. 1541–1558, Mar. 2009.

[35] Q. Chen, D. Baldocchi, G. Peng, and M. Kelly, "Isolating individual trees in a Savanna treeland using small footprint LiDAR data," *Photogramm. Eng. Remote Sens.*, vol. 72, pp. 923–932, Aug. 2006.

[36] D. Panagiotidis, A. Abdollahnejad, P. Surový, and V. Chiteculo, "Determining tree height and crown diameter from high-resolution UAV imagery," *Int. J. Remote Sens.*, vol. 38, pp. 2392–2410.

[37] S. C. Popescu, R. H. Wynne, and R. F. Nelson, "Measuring individual tree crown diameter with LiDAR and assessing its influence on estimating forest volume and biomass," *Can. J. Remote Sens.*, vol. 29, pp. 564–577, Jun. 2003.

[38] I. M. Turner, W. K. Gong, J. E. Ong, and J. S. B. A. Kohyama, "The architecture and allometry of Mangrove saplings," *Funct. Ecol.*, vol. 9, pp. 205–212, Apr. 1995.
[39] W. Wannasiri, M. Nagai, K. Honda, P. Santitamnont, and P. Miphokasap, "Extraction of Mangrove biophysical parameters using airborne LiDAR," *Remote Sens.*, vol. 5, pp. 1787–1808, Apr. 2013.
[40] D. Yin and L. Wang, "Individual mangrove tree measurement using UAV-based LiDAR data: Possibilities and challenges," *Remote Sens. Environ.*, vol. 223, pp. 34–49, Dec. 2019.
[41] L. Wang, P. Gong, and G. S. Biging, "Individual tree-crown delineation and treetop detection in high-spatial-resolution aerial imagery," *Photogramm. Eng. Remote Sens.*, vol. 70, pp. 351–358, Mar. 2004.
[42] Y. Guo, Q. Liu, G. Liu, and C. Huang, "Individual tree crown extraction of high-resolution image based on marker-controlled watershed segmentation method," *J. Geo-Inf. S.*, vol. 18, pp. 1259–1266, Sep. 2016.
[43] H. Huang, X. Li, and C. Chen, "Individual tree crown detection and delineation from very-high-resolution UAV images based on Bias field and marker-controlled watershed segmentation algorithms," *IEEE J. Sel. Top. Appl. Earth Observ. Remote Sens.*, vol. 11, pp. 2253–2262, Mar. 2018.
[44] M. Parkan and D. Tuia, "Estimating uncertainty of point-cloud based individual-tree segmentation with ensemble based filtering," *Remote Sens.*, vol. 10, Feb. 2018, Art. no 335.
[45] J. Hyyppa, O. Kelle, M. Lehikoinen, and M. Inkinen, "A segmentation-based method to retrieve stem volume estimates from 3-D tree height models produced by laser scanners," *IEEE Trans. Geosci. Remote Sens.*, vol. 39, pp. 969–975, Oct. 2001.
[46] A. V. Vo, L. Truong-Hong, D. F. Laefer, and M. Bertolotto, "Octree-based region growing for point cloud segmentation," *ISPRS J. Photogramm.*, vol. 104, pp. 88–100, Mar. 2015.
[47] W. Li, Q. Guo, M. K. Jakubowski, and M. Kelly, "A new method for segmenting individual trees from the LiDAR points cloud," *Photogramm. Eng. Rem S.*, vol. 78, pp. 75–84, Jan. 2012.
[48] M. Alonzo, B. Bookhagen, and D. A. Roberts, "Urban tree species mapping using hyperspectral and LiDAR data fusion," *Remote Sens. Environ.*, vol. 148, pp. 70–83, Mar. 2014.
[49] C. Zhang, Y. Zhou, and F. Qiu, "Individual tree segmentation from LiDAR point clouds for urban forest inventory," *Remote Sens.*, vol. 7, pp. 7892–7913, Jun. 2015.
[50] L. I. Duncanson, B. D. Cook, G. C. Hurtt, and R. O. Dubayah, "An efficient, multi-layered crown delineation algorithm for mapping individual tree structure across multiple ecosystems," *Remote Sens. Environ.*, vol. 154, pp. 378–386, Jul. 2014.
[51] T. Chai and R. R. Draxler, "Root mean square error (RMSE) or mean absolute error (MAE)? – Arguments against avoiding RMSE in the literature," *Geosci. Model Dev.,* vol. 7, pp. 1247–1250, Jun. 2014.
[52] W. Yao, P. Krzystek, and M. Heurich, "Tree species classification and estimation of stem volume and DBH based on individual tree extraction by exploiting airborne full-waveform LiDAR data," *Remote Sens. Environ.*, vol. 123, pp. 368–380.
[53] D. Yin and W. Le, "How to assess the accuracy of the individual tree-based forest inventory derived from remotely sensed data: A review," *Int. J. Remote Sens.*, vol. 37, pp. 4521–4553, Aug. 2016.
[54] L. Wang, "A multi-scale approach for delineating individual tree crowns with very high resolution imagery," *Photogramm. Eng. Remote. Sens.*, vol. 76, pp. 371–378, Apr. 2010.
[55] M. T. Gebreslasie, F. B. Ahmed, J. A. N. V. Aardt, and F. Blakeway, "Individual tree detection based on variable and fixed window size local maxima filtering applied to IKONOS imagery for even-aged Eucalyptus plantation forests," *Int. J. Remote Sens.*, vol. 32, pp. 4141–4154, Aug. 2011.
[56] S. C. Popescu, R. H. Wynne, and R. F. Nelson, "Estimating plot-level tree heights with LiDAR: Local filtering with a canopy-height based variable window size," *Comput. Electron. Agr.*, vol. 37, pp. 71–95, Dec. 2003.
[57] C. Cao *et al.*, "Extraction of forest structural parameters based on the intensity information of high-density airborne light detection and ranging," *J. Appl. Remote. Sens.*, vol. 6, pp. 063533-1–063533-12, Jun. 2012.
[58] C. Edson and M. G. Wing, "Airborne light detection and ranging (LiDAR) for individual tree stem location, height, and biomass measurements," *Remote Sens.*, vol. 3, pp. 2494–2528, Nov. 2011.
[59] M. J. Falkowski *et al.*, "Automated estimation of individual conifer tree height and crown diameter via two-dimensional spatial wavelet analysis of LiDAR data," *Can. J. Remote. Sens.*, vol. 32, pp. 153–161, Nov. 2006.
[60] Z. Zhen, L. Quackenbush, and L. Zhang, "Impact of tree-oriented growth order in marker-controlled region growing for individual tree crown delineation using airborne laser scanner (ALS) data," *Remote Sens.*, vol. 6, pp. 555–579, Jan. 2014.
[61] H. Luo, L. Wang, C. Wu, and L. Zhang, "An improved method for impervious surface mapping incorporating LiDAR data and high-resolution imagery at different acquisition times," *Remote Sens.*, vol. 10, Jun. 2018, Art. no. 1349.

**Tian Yin** received the B.S. degree in geographic information science from Lu dong University, Shandong, China, in 2018. She is currently working toward the M.S. degree in cartography and geography information system with Beijing Forestry University, Beijing, China.

Her research concerns forest parameters extractions by oblique photogrammetry.

**Jian Zeng** received the B.S. degree in forestry from Central South University of Forestry and Technology, Hunan, China, in 2016, and the M.S. degree in cartography and geographic information system from Beijing Forestry University, Beijing, China, in 2019.

From 2019 to 2020, he was with China Siwei Surveying and Mapping Technology Company Ltd, Beijing, China.

His research concerns forest parameters extractions and 3-D reconstruction by oblique photogrammetry.

**Xiaoli Zhang** (Member, IEEE) received the B.S. degree in computer science from He Bei University, Baoding, China, in 1989 and the Ph.D. degree in forest management science from Beijing Forestry University, Beijing, China, in 1998.

From 2006 to 2007, she was a Visiting Scholar in remote sensing and intelligent analysis with Lincoln University, New Zealand.

From 1989 to 1992, she was an Assistant with the Mathematics Department, Zhangjiakou Normal College, Hebei province, China. From 1998 to 1999, she was a Postdoctoral Research Fellow with the Institute of Remote Sensing Application in CAC, Beijing, China. From 1999 to 2006, she was an Associate professor with the College of Forestry, Beijing Forestry University, Beijing, China, and since 2007, she had been a Professor. Her research interests include forest resources and ecological environment remote sensing monitoring and spatial prediction, forest disease and pest remote sensing monitoring and risk assessment, and vegetation quantitative remote sensing.

Prof. Zhang is a Councilor of the Associate on Environment Remote Sensing of China, a Supervisor of Beijing Society for Information Technology in Agriculture and a member of Forest Management Branch of Chinese Society of Forestry. His awards and honors include The National Scientific and Technological Progress Award, MOE Scientific and Technological Progress Award, Beijing Science and Technology Award, Forest Science & Technology Award for Chinese Youth and MOE New Century Excellent Talents.

**Xuemei Zhou** received the B.S. degree in geographic information science from Anhui Normal University, Anhui, China, in 2017 and the M.S. degree in cartography and geographic information system from Beijing Forestry University, Beijing, China.

Her research concerns forest parameters extractions by oblique photogrammetry.